2017

Development and Physicochemical Characterization of Acetalated Dextran Aerosol Particle Systems for Deep Lung Delivery

Zimeng Wang
University of Rhode Island

Sweta K. Gupta
University of Rhode Island

See next page for additional authors

Citation/Publisher Attribution
Wang, Z., Gupta, S. K., & Meenach, S. (2017). Development and Physicochemical Characterization of Acetalated Dextran Aerosol Particle Systems for Deep Lung Delivery. *International Journal of Pharmaceutics, 525*(1), 264-274. doi:10.1016/j.ijpharm.2017.04.052
Available at: http://dx.doi.org/10.1016/j.ijpharm.2017.04.052

Development and Physicochemical Characterization of Acetalated Dextran Aerosol Particle Systems for Deep Lung Delivery

Zimeng Wang[1], Sweta K. Gupta[1], Samantha A. Meenach[1,2]

[1]University of Rhode Island, College of Engineering, Department of Chemical Engineering, Kingston, RI 02881, USA

[2]University of Rhode Island, College of Pharmacy, Department of Biomedical and Pharmaceutical Sciences, Kingston, RI 02881, USA

Corresponding Author: Samantha A. Meenach, University of Rhode Island, 205 Crawford Hall, 16 Greenhouse Road, Kingston, RI, 02881, USA. Email: smeenach@uri.edu

ABSTRACT

Biocompatible, biodegradable polymers are commonly used as excipients to improve the drug delivery properties of aerosol formulations, in which acetalated dextran (Ac-Dex) exhibits promising potential as a polymer in various therapeutic applications. Despite this promise, there is no comprehensive study on the use of Ac-Dex as an excipient for dry powder aerosol formulations. In this study, we developed and characterized pulmonary drug delivery aerosol microparticle systems based on spray-dried Ac-Dex with capabilities of (1) delivering therapeutics to the deep lung, (2) targeting the particles to a desired location within the lungs, and (3) releasing the therapeutics in a controlled fashion. Two types of Ac-Dex, with either rapid or slow degradation rates, were synthesized. Nanocomposite microparticle (nCmP) and microparticle (MP) systems were successfully formulated using both kinds of Ac-Dex as excipients and curcumin as a model drug. The resulting MP were collapsed spheres approximately 1 μm in diameter, while the nCmP were similar in size with wrinkled surfaces, and these systems dissociated into 200 nm nanoparticles upon reconstitution in water. The drug release rates of the Ac-Dex particles were tuned by modifying the particle size and ratio of fast to slow degrading Ac-Dex. The pH of the environment was also a significant factor that influenced the drug release rate. All nCmP and MP systems exhibited desirable aerodynamic diameters that are suitable for deep lung delivery (e.g. below 5 μm). Overall, the engineered Ac-Dex aerosol particle systems have the potential to provide targeted and effective delivery of therapeutics into the deep lung.

KEYWORDS: Acetalated dextran, nanocomposite microparticles, microparticles, pulmonary delivery, spray drying, controlled release

1. INTRODUCTION

Pulmonary drug delivery has exhibited promising potential in the treatment of lung diseases, as it allows for the delivery of a wide range of therapeutics directly and efficiently to the lungs, thereby increasing local drug concentration, reducing systemic side effects, providing a rapid onset of pharmaceutical action, and avoiding the first-pass metabolism associated with the liver (Belotti et al., 2015; Cui et al., 2011; Mansour et al., 2009; Meenach et al., 2012). The deep lung (alveolar) region can be utilized as a route for systematic drug delivery due to the enormous surface area available and nearby plentiful capillary vessels that facilitate drug absorption, the very thin (approximately 0.1 μm) liquid layer over the alveoli that ensures rapid and unhindered drug absorption, and low enzymatic activity, which enhances drug availability (Collier et al., 2016; Cui et al., 2011; Hoang et al., 2014). As a result, various therapeutics such as antibiotics, proteins, peptides, anti-cancer drugs (Wu et al., 2014), plasmid DNA (Takashima et al., 2007), siRNA (Jensen et al., 2010), and anti-tuberculosis (TB) drugs have been employed in inhalation formulations for the treatment of pulmonary diseases such as asthma, chronic obstructive pulmonary disease (COPD), cystic fibrosis (CF)-related pulmonary infections, and lung cancer (Meenach et al., 2013a; Wu et al., 2014).

Dry powders are a dosage formulation that delivers therapeutics to the lung, in the form of particles, using a dry powder inhaler (Wu et al., 2014). Compared with liquid aerosols, these formulations offer additional benefits such as enhanced stability of the

formulation, controllable particle size for targeting different regions of the lung, and increased drug loading of hydrophobic payloads (Cohen et al., 2010; Meenach et al., 2013a). Spray drying has proven to be a suitable technology in the preparation of dry powder therapeutics (Meenach et al., 2013a), as it is capable of producing respirable microparticles for deep lung delivery with acceptable aerosol dispersion properties (Belotti et al., 2015). Properties of dry powder particles such as particle size, particle shape, and surface morphology can be modified by controlling the spray drying production process, thus providing desirable particle characteristics (Belotti et al., 2015; Wu et al., 2014).

Biocompatible, biodegradable polymers such as poly(ε-caprolactone) (PCL) and poly(lactic-co-glycolic acid) (PLGA) have been used as dry powder formulation excipients to carry drug molecules, protect drugs from degradation, and impart sustained release to aerosol formulations (Mansour et al., 2009). However, PLGA and PCL delivery systems show significant burst release of their payloads due to bulk erosion of the polymers and it is difficult to control the polymer degradation rate and modulate their release profiles (Ulery et al., 2011). Acetalated dextran (Ac-Dex) is an acid-sensitive, biodegradable, biocompatible polymer prepared via a one-step reaction by reversibly modifying dextran with acetal groups. This modification reverses the solubility properties of dextran from hydrophilic to hydrophobic, making it possible to form polymeric particles using standard emulsion or nanoprecipitation techniques. In contrast to other commonly used polymers such as PLGA, polylactic acid, and PCL, Ac-Dex exhibits attractive properties suitable for the controlled release of therapeutic payloads. By controlling the reaction time during the formation of Ac-Dex, the ratio of cyclic acetal

groups (with a slower degradation rate) to acyclic acetal groups (with a faster degradation rate) can be adjusted. As a result, the degradation rate of the resulting Ac-Dex can be tuned from hours to months to suit various applications. Moreover, the acid-sensitivity of Ac-Dex enables it to degrade faster in lower pH environments, such as lysosomes in macrophage or tumor cells, allowing for controlled release of drug within these cells. Furthermore, Ac-Dex degrades into neutral by-products, which avoids undesirable changes in the micro-environmental pH in the body. Finally, Ac-Dex offers the potential of targeted delivery, due to the presence of dextran chains that can be further modified with a variety of functional targeting moieties (Bachelder et al., 2008; Broaders et al., 2009; Kauffman et al., 2012).

Owing to the aforementioned advantages, Ac-Dex has been widely applied in the formation of polymeric carriers for drug delivery. Porous Ac-Dex microparticles loaded with the chemotherapeutic camptothecin were developed for pulmonary delivery using emulsion techniques. These systems exhibited a respirable fraction of 37% and experimental mass mean aerodynamic diameters from 5.3 - 11.9 μm (Meenach et al., 2012). Ac-Dex nanoparticle systems have been investigated in the application of protein delivery for immunotherapy (Broaders et al., 2009), gene delivery to phagocytic and non-phagocytic cells (Cohen et al., 2010), tandem delivery of peptide and chemotherapeutic for controlled combination chemotherapy (Cui et al., 2011), delivery of the host-mediated compound AR-12 (Arno Therapeutics; formerly known as OSU-03012) for the treatment of Leishmania donovani (Collier et al., 2016), and the control of Salmonella infections (Collier et al., 2016). Both Ac-Dex nanoparticles and microparticles loaded with

123 horseradish peroxidase have been evaluated to improve vaccine stability outside cold
124 chain conditions (Kanthamneni et al., 2012).

125 Despite this work, there is no comprehensive study on using Ac-Dex as an
126 excipient for dry powder aerosol formulations produced via spray drying. In this study,
127 we aimed to develop and characterize dry powder pulmonary delivery systems based on
128 spray-dried Ac-Dex particles with capabilities of (a) delivering therapeutics to the deep
129 lung, (b) targeting the particles to a particular location within the lungs, and (c) releasing
130 therapeutics at a controlled rate. Previous studies have shown that: (a) aerodynamic
131 diameter (d_a) determines the region of the lungs where particles will deposit, where
132 particles with an d_a of 1 - 5 μm tend to deposit in the deep lung region (Meenach et al.,
133 2013a); (b) geometric size plays an important role in the cellular uptake of particles,
134 where nanoscale particles (approximately 150 nm) tend to escape phagocytic uptake (He
135 et al., 2010), while particles larger than 1 μm will suffer from macrophage clearance in
136 the alveoli (Kho et al., 2010); and (c) the drug release rate of Ac-Dex particles can be
137 tuned by modifying the synthesis time of the Ac-Dex polymer (Kauffman et al., 2012;
138 Meenach et al., 2012).

139 To prepare the engineered particle systems, two types of Ac-Dex with rapid or
140 slow degradation rates were synthesized. Nanocomposite microparticle (nCmP) and
141 microparticle (MP) systems were formulated using both kinds of Ac-Dex as the
142 excipient. Curcumin was used as model drug owing to its high hydrophobicity (similar to
143 many other pulmonary therapeutics) and fluorescence (allowing for easy detection). The
144 nCmP were prepared by spray drying an aqueous suspension of CUR-loaded Ac-Dex
145 nanoparticles (NP, 200 nm) and the solid MP were formulated by spray drying a solution

of Ac-Dex and CUR in a solution of tetrahydrofuran (THF) and acetone. We hypothesize that upon pulmonary administration, the nCmP will deposit in the deep lung, decompose into free NP, and facilitate the sustained release of drug to the targeted site, while the MP will remain the original size after deposition in the deep lung region. A schematic of the described particle preparation and design is shown in **Figure 1.** Overall, the goal of the described research was the initial development and physicochemical characterization of dry powder Ac-Dex aerosol particle systems with the potential for effective delivery of therapeutics.

2. MATERIALS AND METHODS

2.1 Materials

Dextran from Leuconostoc mesenteroides (9000-11000 MW), pyridinium p-toluenesulfonate (PPTS, 98%), 2-methoxypropene (2-MOP, 97%), triethylamine (TEA, ≥ 99%), anhydrous dimethyl sulfoxide (DMSO, ≥ 99.9%), poly(vinyl alcohol) (PVA, MW 13,000-23,000, 87-89% hydrolyzed), dichloromethane (DCM, anhydrous, ≥ 99.8%), deuterium chloride (DCl, 35 weight % in D_2O, 99 atom % D), Tween® 80, curcumin, sodium acetate (≥ 99%), acetic acid solution (1.0 N), acetone (≥ 99.8%), tetrahydrofuran (THF, ≥ 99%), and methanol (anhydrous, ≥ 99.9%) were obtained from Sigma–Aldrich (St. Louis, MO). Deuterium oxide (D_2O, 99.8% atom D) was obtained from Acros Organics (Geel, Belgium). Phosphate buffered saline (PBS) was obtained from Fisher Scientific (Somerville, NJ). Hydranal® KF reagent was obtained from Fluka Analytical.

2.2 Synthesis and NMR Analysis of Acetalated Dextran (Ac-Dex)

Ac-Dex was synthesized as described previously (Bachelder et al., 2008) with minor modifications. 1 g of lyophilized dextran and 25 mg of PPTS were dissolved in 10 mL of anhydrous DMSO. The resulting solution was reacted with 5 mL of 2-MOP under nitrogen gas for 5 minutes to prepare Ac-Dex with a rapid degradation rate (Ac-Dex-5min) or for 3 hours to prepare Ac-Dex with a slower degradation rate (Ac-Dex-3h). The reaction was quenched with 1 mL of TEA. The reaction mixture was then precipitated in basic water (water and TEA, pH 9), vacuum filtered, and lyophilized (−50 °C, 0.023 mbar) for 24 hours to yield a solid product.

The cyclic-to-acyclic (CAC) ratio of acetal coverage and degrees of total acetal coverage per 100 glucose molecules was confirmed by ^{1}H NMR spectroscopy (Bruker 300 MHz NMR, MA). 10 mg of Ac-Dex was added to 700 μL of D_2O and was hydrolyzed with 30 μL of DCl prior to analysis. The hydrolysis of one cyclic acetal group produces one acetone molecule whereas one acyclic acetal produces one acetone and one methanol molecule each. Consequently, from the normalized integration of peaks related to acetone, methanol, and the carbon ring of dextran, the CAC ratio of acetal coverage and degrees of total acetal coverage per 100 glucoses were determined.

2.3 Formation of CUR-Loaded Ac-Dex Nanoparticles (CUR NP)

Curcumin-loaded nanoparticles (CUR NP) were prepared via an oil/water emulsion solvent evaporation using Ac-Dex-5min, Ac-Dex-3h, or a mixture of both types of Ac-Dex (50 % w/w). 49 mg of Ac-Dex and 1 mg of CUR were dissolved in 1 mL of DCM over an ice bath, establishing the organic phase. The aqueous phase was comprised

of 6 mL of 3% PVA in PBS and was added to the organic phase. The resulting mixture was sonicated (Q500 Sonicator, Qsonica, Newtown, CT) for 30 seconds with a 1 second on/off pulse at 70% amplitude. The emulsion was transferred to a spinning solution of 0.3% PVA in PBS and was stirred for 3 hours to allow for evaporation of the organic solvent and particle hardening. The solution was then centrifuged at 19802 ×g for 20 minutes to collect the nanoparticles. Nanoparticles were washed once with DI water, redispersed in 0.1% PVA, and lyophilized (−50 °C, 0.023 mbar) for 48 hours. The resulting NP systems were: CUR NP-5min (made of Ac-Dex-5min only), CUR NP-3h (made of Ac-Dex-3h only), and CUR NP-h (50 wt% Ac-Dex-5min and 50 wt% Ac-Dex-3h).

2.4 Formulation of CUR Nanocomposite Microparticles (CUR nCmP) via Spray Drying

CUR nCmP were prepared via the spray drying of an aqueous suspension of each type of CUR NP (0.5%, w/v) using a Büchi B-290 spray dryer (Büchi Labortechnik, AG, Switzerland) in open mode. The CUR NP suspension was sonicated for 10 minutes before spray drying. The spray drying conditions were as follows: inlet temperature of 60 °C (outlet temperature of 32 ± 2 °C), 0.7 mm nozzle diameter, atomization gas flow rate of 414 L/h using dry nitrogen, aspiration rate of 28 m^3/h, pump rate of 0.9 mL/min, and nozzle cleaner rate of 3. The resulting nCmP were separated in a high-performance cyclone, dried for 15 minutes in the spray dryer for further removal of residual water, collected in a sample collector, and stored in amber glass vials in a desiccator at −20°C.

nCmP comprised of each kind of NP described previously were produced: nCmP-5min, nCmP-3h, and nCmP-h, correspondingly.

2.5 Formulation of CUR Microparticles (CUR MP) via Spray Drying

Solid curcumin-loaded microparticles (CUR MP) were prepared via the spray drying of an organic solution comprised of Ac-Dex and CUR using a Büchi B-290 spray dryer in closed mode. The organic solutions were prepared by dissolving CUR and Ac-Dex (2:98 w/w) in an organic solvent comprised of 85% acetone and 15% THF (v/v) at a solids concentration of 2% (w/v). The spray drying conditions were as follows: inlet temperature of 60 °C (outlet temperature of 40 ± 2 °C), 0.7 mm nozzle diameter, atomization gas flow rate of 414 L/h using UHP dry nitrogen, aspiration rate of 40 m^3/h, pump rate of 3 mL/min, and nozzle cleaner rate of 0. The resulting MP were separated in a high-performance cyclone, dried for 15 minutes in the spray dryer for further removal of residual solvent, collected in a sample collector, and stored in amber glass vials in a desiccator at −20°C. The resulting MP were: MP-5min (from Ac-Dex-5min), MP-3h (from Ac-Dex-3h), and MP-h (from 50 wt% Ac-Dex-5min and 50 wt% Ac-Dex-3h).

2.6 Particle Size, Size Distribution, and Zeta Potential Analysis

The average diameter, size distribution, and zeta potential of the original NP and the NP released from the dispersion of nCmP in water were measured by dynamic light scattering (DLS) using a Malvern Nano Zetasizer (Malvern Instruments, Worcestershire, UK). The original NP and nCmP were dispersed in DI water (pH = 7, 0.3 mg/mL) prior

to analysis. All experiments were performed in triplicate with a scattering angle of 173° at 25 °C.

2.7 Particle Morphology and Shape Analysis via Scanning Electron Microscopy (SEM)

The shape and surface morphology of the nCmP and MP were evaluated by SEM using a Zeiss SIGMA VP Field Emission-Scanning Electron Microscope (FE-SEM) (Germany). Particle samples were placed on aluminum SEM stubs (Ted Pella, Inc., Redding, CA) with double-sided adhesive carbon tabs. The samples were coated with a thin film of a gold/palladium alloy using a BIO-RAD sputter coating system at 20 μA for 60 seconds under argon gas. Images were captured at 8 kV at various magnifications. The geometric mean diameter and standard deviation of the MP were measured digitally from SEM images using ImageJ software (Rasband, 1997-2016). Representative micrographs (5000x magnification) for each sample were analyzed by measuring the diameter of at least 300 particles.

2.8 Tapped Density Evaluation of nCmP and MP

The tapped density of the particles was measured as described previously with minor modifications (Tomoda et al., 2008). 35 - 40 mg of particles was weighed into a glass tube. The tube was tapped 200 times to ensure efficient packing of the particles and then the volume occupied by the particles was measured using calipers. The density of the particles was then determined by the following equation:

$$\rho = \frac{m}{V} \quad (1)$$

where ρ is the tapped density, m is the particle mass, and V is the volume occupied by the particles as determined by measuring the height of the particles in the tube with a known diameter (5 mm). The theoretical mass median aerodynamic diameter ($MMAD_T$) of the particles was then calculated using the following equation:

$$MMAD_T = d\sqrt{\frac{\rho}{\rho^*}} \quad (2)$$

where d is the geometric diameter determined by ImageJ, ρ is the tapped density of the particles, and $\rho^* = 1$ g/cm^3, which is the reference density of solid polymer.

2.9 Drug Loading Analysis of nCmP and MP

The drug loading and encapsulation efficiency of CUR nCmP and CUR MP were determined via fluorescence spectroscopy (Biotek Cytation 3, Winooski, VT). All particle samples were dissolved in DMSO and were evaluated at 420 nm (excitation) and 520 nm (emission). The CUR drug loading and encapsulation efficiency (EE) of the particles were determined by the following equations:

$$\text{Drug loading} = \frac{\text{mass of CUR loaded in particles}}{\text{mass of particles}} \quad (3)$$

$$\text{Encapsulation efficiency (EE)} = \frac{\text{mass of CUR loaded in particles}}{\text{initial mass of CUR in particles}} \times 100\% \quad (4)$$

279

280 **2.10 *In Vitro* Drug Release from nCmP and MP**

281 The *in vitro* release profiles of CUR from nCmP and MP were determined via the
282 release of suspended particles (0.5 mg/mL, 1.5 mL) in modified phosphate buffer (0.1 M,
283 pH = 7.4, 0.5 wt% Tween® 80) and modified acetate buffer (0.1 M, pH = 5, 0.5 wt%
284 Tween® 80). The particle suspensions were incubated at 37 °C and 100 rpm (Digital Heat
285 Block and ORBi shaker, Benchmark Scientific, Edison, NJ). At various time points,
286 particle samples were centrifuged at 23102 ×g for 5 minutes at 4 °C to isolate the NP.
287 200 μL of supernatant was withdrawn and replaced by the same amount of fresh modified
288 buffer in each sample. The withdrawn solutions were mixed with an equal volume of
289 DMSO and analyzed for CUR content via fluorescence spectroscopy using the same
290 method described for drug loading. The release data was fitted to several commonly
291 utilized drug release models (Supplemental Information **Section S.1**) to elucidate the
292 mechanism of drug release of Ac-Dex particles. The coefficient of determination (R^2)
293 was applied to test the applicability of the described release models.

294

295 **2.11 Differential Scanning Calorimetry (DSC)**

296 The thermal phase transitions of nCmP, MP, and their raw components were
297 determined via DSC using a TA Q10 DSC system (TA Instruments, New Castle, DE,
298 USA) equipped with an automated computer-controlled TA instruments DSC refrigerated
299 cooling system. 1 - 3 mg of sample was weighed into Tzero™ alodine-coated aluminum
300 pans that were hermetically sealed. The sealed pans were placed into the DSC furnace

along with an empty sealed reference pan. The heating range was 0 – 200 °C at a heating rate of 10 °C/min.

2.12 Powder X-Ray Diffraction (PXRD)

The crystalline states of nCmP, MP, and its raw components were examined by PXRD using a Rigaku Multiflex X-ray diffractometer (The Woodlands, TX) with a Cu Kα radiation source (40 kV, 44 mA). The samples were placed on a horizontal quartz glass sample holder (3 mm) prior to analysis. The scan range was 5 – 60° in 2Θ with a step width of 0.1 and scan rate of 1 °/min.

2.13 Karl Fischer Coulometric Titration

The water content of nCmP and MP was quantified by Karl Fischer (KF) titration using a 737 KF coulometer (Metrohm, Riverview, FL). 5 mg of powder was dissolved in anhydrous methanol. The resulting solution was injected into the KF reaction cell filled with Hydranal® KF reagent and then the amount of water was analyzed. Pure solvent was also injected for use as a background sample.

2.14 *In Vitro* Aerosol Dispersion Performance with the Next Generation Impactor (NGI)

In vitro aerosol dispersion performance of nCmP and MP was evaluated using a Next Generation Impactor™ (NGI™, MSP Corporation, Shoreview, MN) equipped with a stainless steel induction port (USP throat adaptor) attachment and stainless steel gravimetric insert cups. The NGI™ was coupled with a Copley TPK 2000 critical flow

controller, which was connected to a Copley HCP5 vacuum pump (Copley Scientific, United Kingdom). The air flow rate (Q) was measured and adjusted to 60 L/min before each experiment in order to model the flow rate in a healthy adult lung. Glass fiber filters (55 mm, Type A/E, Pall Life Sciences, PA) were placed in the gravimetric insert cups for stages 1 through 7 to minimize particle bounce or re-entrapment (Meenach et al., 2013a) and these filters were weighed before and after the experiment to determine the particle mass deposited on each stage. Approximately 10 mg of powder was loaded into a hydroxypropyl methylcellulose (HPMC, size 3, Quali-V®, Qualicaps® Inc., Whitsett, NC, USA) capsule and the capsule was placed into a human dry powder inhaler device (HandiHaler, Boehringer Ingelheim Pharmaceuticals, CT) attached to a customized rubber mouthpiece connected to the NGI™. Three HPMC capsules were loaded and released in each measurement and experiments were performed in triplicate. The NGI™ was run with a delay time of 10 s and running time of 10 s. For Q = 60 L/min, the effective cutoff diameters for each stage of the impactor were given from the manufacturer as: stage 1 (8.06 μm); stage 2 (4.46 μm); stage 3 (2.82 μm); stage 4 (1.66 μm); stage 5 (0.94 μm); stage 6 (0.55 μm); and stage 7 (0.34 μm). Our previous study on the relationship between particle mass distribution and payload distribution showed that no significant difference existed between the drug amount and particle mass in each chamber of NGI ($p > 0.05$), indicating that the drug was uniformly dispersed in both CUR-MP and CUR-nCmP (**Figure S1**). The fine particle fraction (FPF), respirable fraction (RF), and emitted dose (ED) were calculated as follows:

$$\text{Fine particle fraction (FPF)} = \frac{\text{mass of particles on Stages 2 through 7}}{\text{initial particle mass loaded into capsules}} \times 100\% \quad (5)$$

345

$$\text{Respirable fraction (RF)} = \frac{\text{mass of particles on Stages 2 through 7}}{\text{total particle mass on all stages}} \times 100\% \quad (6)$$

$$\text{Emitted dose (ED)} = \frac{\text{initial mass in capsules - final mass remaining in capsules}}{\text{initial mass in capsules}} \times 100\% \quad (7)$$

346

347 The experimental mass median aerodynamic diameter ($MMAD_E$) and geometric
348 standard deviation (GSD) for the particles were determined using a Mathematica®
349 program written by Dr. Warren Finlay (Meenach et al., 2013a; W, 2008).

350

351 **2.15 Statistical Analysis**

352 All measurements were performed in at least triplicate. Values are given in the
353 form of mean ± standard deviation. The statistical significance of the results was
354 determined using analysis of variance (ANOVA) and student's t-test. A p-value of <0.05
355 was considered statistically significant.

356

357 **3. RESULTS AND DISCUSSION**

358

359 **3.1 Preparation and Characterization of Ac-Dex and Curcumin Nanoparticles**

360

361 *3.1.1 NMR Analysis of Ac-Dex*

362 Successful synthesis of Ac-Dex was confirmed by ^{1}H NMR (**Figure S2**). Ac-Dex-
363 5min exhibited 61.2% cyclic acetal coverage (CAC) and 71.6% total conversion of -OH

groups, while Ac-Dex-3h exhibited 82.5% CAC and 80.0% total conversion of -OH groups, which matched our previous results (Wang et al., 2016; Wang and Meenach, 2016). The Ac-Dex with longer synthesis time (Ac-Dex-3h) exhibited a higher CAC, which was in accordance with previous studies. An increase in CAC is known to decrease polymer degradation and ultimately, the drug release rate, due to the slower degradation of the cyclic acetal groups on the Ac-Dex backbone (Bachelder et al., 2008; Broaders et al., 2009). Ac-Dex-3h also showed a higher total conversion of -OH groups, which could be a result the longer reaction time. This higher total acetal coverage is favorable in the enhancement of the stability of the PVA coating of nanoparticles (data not shown), thus ensuring small particle size and narrow size distribution.

3.1.2 Dynamic Light Scattering (DLS) Analysis of Original and Redispersed CUR NP

Average nanoparticle size, size distribution/polydispersion index (PDI), and zeta potential are shown in **Table 1.** No significant changes in NP size, PDI, or zeta potential was found between the original and redispersed NP ($p < 0.05$), indicating that the CUR NP maintained their properties after redispersion. The original and redispersed NP exhibited an average diameter of approximately 200 nm, which is in the desirable range to avoid macrophage clearance and mucus entrapment (Kho et al., 2010). The low PDI value denotes a narrow size distribution of the NP, and the slightly negatively charged surface of nanoparticles, as measured by zeta potential, is desirable in order to reduce the interactions with negatively charged mucin fibers present in airway mucus (Lai et al., 2009). According to our preliminary experiments (data not shown), a low total conversion of -OH groups on the Ac-Dex results in NP with larger sizes and PDI due to

NP agglomeration. This phenomenon could be a result of the reduced hydrophobicity of Ac-Dex with fewer -OH groups converted to acetal groups, which leads to insufficient absorption of PVA on the NP surface. However, the Ac-Dex in this study was prepared to produce NP with small sizes and low PDI, as the total conversion of -OH groups was kept in a higher range to prevent NP agglomeration.

3.2 Preparation and Characterization of Nanocomposite Microparticles (nCmP) and Microparticles (MP)

3.2.1 Morphology, Sizing, and Size Distribution

CUR nCmP displayed a wrinkled surface with visibly encapsulated NP as seen in **Figure 2 and Figure S3**. The raisin-like morphology of the nCmP can be attributed to the early formation of nanoparticle shells in the solution droplets during spray drying, which determines the geometric size of nCmP. As the drying process proceeds, the remaining solvent evaporates from the droplet center, resulting in hollow particles that tend to shrink (Atalar and Dervisoglu, 2015; Gu et al., 2015).

CUR MP were collapsed, wrinkled spheres as seen in **Figures 2D-F**. Altering the Ac-Dex composition of the particles had no impact on particle morphology. The geometric diameters (d_g) of the CUR nCmP and MP systems are shown in **Table 2**. All of the MP d_g were approximately 1 μm in size, which is reported to make the particles vulnerable to macrophage uptake (Sung et al., 2009). In contrast, the NP released from nCmP systems can escape macrophage clearance upon reaching the deep lung.

410 *3.2.2 Analysis of Particle Density*

411 The density of the particles was determined via tapped density measurements, as
412 shown in **Table 2**. CUR nCmP exhibited tapped density values around 0.12 g/cm^3, while
413 the MP system showed values around 0.05 g/cm^3. These density values are relatively low
414 compared with the raw materials (~1 g/cm^3), which can be attributed to the wrinkled
415 morphology and hollow structures of the particle systems. It has been reported that
416 particles > 1 μm in diameter with greater density will deposit in the lungs by
417 sedimentation (Heyder, 2004). Therefore, the increased density of CUR nCmP system as
418 compared to MP could enhance their rate of deposition into the deep lung.

419

420 *3.2.3 Loading and In Vitro Release of CUR*

421 CUR was successfully encapsulated into both the nCmP and MP systems as seen
422 in **Table 2**. The MP systems prepared via closed mode, organic spray drying exhibited
423 higher encapsulation efficiency (EE, > 50%) than the nCmP systems (approximately
424 30%) prepared in open mode in aqueous solutions. The lower EE of the nCmP can be
425 attributed to the EE of the original CUR-loaded NP, which was also approximately 30%
426 (**Table S1**). The spray drying process had no influence on the CUR loading and EE for
427 the nCmP systems ($p < 0.05$), which indicates that the drug loading of nCmP systems can
428 be determined during NP preparation.

429 Results of the *in vitro* release of CUR from both nCmP and MP systems in
430 modified phosphate (pH 7.4) and acetate (pH 5) buffers at physiological temperature
431 (37°C) are reported in **Figure 3** as the percentage of cumulative drug released over time.
432 As shown in **Table S2**, the particle systems exhibited shorter release durations and

433 increased release of CUR ($p < 0.05$) at acidic pH with the exception of nCmP-5min,
434 which only exhibited a shorter release duration. These results are in accordance with
435 previous studies (Meenach et al., 2012; Vehring, 2008). The release profiles suggest that
436 the drug will be released at significantly higher rates once the carrier particles reach an
437 acidic environment. This can allow Ac-Dex particles the ability to provide controlled
438 release of a therapeutic payload in cells and tissue with lower pH values, such as tumor
439 cells and macrophages. In contrast, if the carrier particles remain in the extracellular or
440 neutral pH environments, the release rate can be reduced, which can minimize systemic
441 and local cytotoxicity (Meenach et al., 2012).

442 In addition, the nCmP systems exhibited faster release than the MP systems,
443 which is likely due to the larger surface area available in the nano-sized delivery systems.
444 Upon reaching an aqueous environment, the nCmP dissociate into nanoparticles with
445 large surface areas and a PVA coating that facilitates particle dispersity, while the MP
446 may agglomerate due to their highly hydrophobic, uncoated surfaces. As a result, the
447 nCmP systems undergo faster polymer degradation and drug diffusion, resulting in a
448 faster release of payloads than MP at both acidic and physiologic pH.

449 Particles comprised of Ac-Dex-3h exhibited slower release rates than those
450 comprised of Ac-Dex-5min, indicating that the drug release rate can be controlled by the
451 polymer reaction time. At pH 7.4, particles made of Ac-Dex-h exhibited a drug release
452 rate between Ac-Dex-5 min and Ac-Dex-3h, suggesting that the ratio of different types of
453 Ac-Dex can also act as an important factor in adjusting the release profiles of particle
454 systems. Nevertheless, the drug release rates of the Ac-Dex particles at pH 5 did not
455 follow this trend, which could be explained by one of the following: (1) the release

profile of Ac-Dex particles is polymer degradation controlled and the decomposition of the Ac-Dex matrix is greatly impacted by the release buffer pH and (2) the release profile of Ac-Dex particles is both polymer degradation and drug diffusion controlled. In previous studies, drug release from Ac-Dex particles was associated with Ac-Dex degradation (Bachelder et al., 2008; Kauffman et al., 2012; Meenach et al., 2012). However, Ac-Dex degradation may result in the surface erosion of particles, formation of large pores in the particles that facilitate drug diffusion, or both at the same time. As a result, the drug release profile could be controlled by drug diffusion through water-filled pores (diffusion controlled), polymer erosion on the particle surface (erosion controlled), or both drug diffusion and surface erosion (diffusion and erosion controlled), respectively (Broaders et al., 2009).

In order to further illustrate the mechanism of drug release of Ac-Dex particles, we fitted the CUR release data to several commonly utilized drug release models, including: (1) a first order model and (2) Hixson–Crowell model for drug dissolution-controlled release, (3) Higuchi model modified to fit burst release at time 0, (4) Korsmeyer–Peppas model and (5) Baker–Lonsdale for drug diffusion-controlled release, (6) Hopfenberg model for surface erosion-controlled release, (7) Baker's model for both degradation and diffusion-controlled release, and (8) Weibull model as a general empirical equation to describe a dissolution or release process (Bohrey et al., 2016; Costa and Sousa Lobo, 2001; Kamaly et al., 2016; Seidlitz and Weitschies, 2012; Shuwisitkul, 2011). The coefficient of determinations (R^2) of the fit for the models are summarized in **Table S3**. The modified Higuchi and Baker–Lonsdale models exhibited higher R^2 compared with other models, indicating that the drug release profiles of all Ac-Dex

particles at both acidic and neutral pH was due primarily to drug diffusion. For Baker's model (Shuwisitkul, 2011) that describes a degradation and diffusion process, the optimal coefficient k was 0, thus the equation of Baker's model exhibited the same form as the equation for the Higuchi model. Since the degradation of Ac-Dex was observable during the release experiments, the release profiles of Ac-Dex particles can be explained by the mechanism of drug diffusion through water-filled pores (Kamaly et al., 2016). In the process of drug diffusion through water-filled pores, water was absorbed by Ac-Dex particles and filled in the pores of the polymer matrix, through which the drug diffused into the buffer. As polymer degraded, both pore size and number increased, resulting in enhanced drug release. Therefore, the reaction time of Ac-Dex affected the drug release rate significantly by controlling the formation of pores of particle matrix but not polymer degradation on the surface. Meanwhile, the water absorption into the particles may also influence the drug release rate, which can be supported by the fact that Ac-Dex-3h had a higher ratio of total hydrophobic acetalated group conversion than Ac-Dex-5min. The fitted release curves using modified Higuchi model are shown in **Figure S4** along with the original data points. The model was modified to fit the burst release at time 0 of the particle systems, which can be attributed to CUR being initially available on the surface of the particles. The nCmP systems exhibited a high release at time 0 because the nanoparticle suspension was sonicated before spray drying to form a uniform dispersion, which may cause CUR release in to the suspension.

3.3.4 Karl Fischer Titration

The residual water content of CUR nCmP and MP is shown in **Table 2**. The water content of nCmP system was approximately 8%, while that of MP system was approximately 6%. The lower water content of MP samples is likely due to the absence of water during the closed mode spray drying process. All particle systems showed acceptable water content for aerosol formulations. In general, reducing the water content in inhalable dry powders can significantly improve their dispersion properties and enhance the stability of the powders during storage (Hickey et al., 2007; Mohammadi et al., 2010). Correspondingly, low water content in inhalable dry powders is highly favorable for efficient dry powder aerosolization and effective particle delivery (Mohammadi et al., 2010; Wu et al., 2013).

3.3.5 Differential Scanning Calorimetry

Figure 4 shows DSC thermograms of the raw materials used in particle preparation and the final CUR nCmP and CUR MP systems. Both the raw Ac-Dex-5min and Ac-Dex-3h displayed endothermic phase transition peaks due to melting (T_m) near 170 °C. The peaks were broad because of the wide size distribution of Ac-Dex polymer crystallites. None of the CUR nCmP systems exhibited a peak corresponding to Ac-Dex melting, which indicates that the Ac-Dex was transformed in an amorphous state by rapid precipitation during NP formation. The CUR MP systems exhibited broad phase transition peaks near 160 °C, which corresponds to the melting of Ac-Dex. This phase transition shifted to the lower temperature range, indicating a reduction in the crystallinity of Ac-Dex after the spray drying process.

524 *3.3.6 Powder X-ray Diffraction (PXRD)*

525 X-ray diffraction diffractograms of the raw materials, physical mixture of Ac-Dex
526 and CUR, CUR nCmP, and CUR MP are shown in **Figure 5**. No peaks were present for
527 either raw Ac-Dex samples, suggesting an irregular distribution or lack of Ac-Dex
528 crystallites. The absence of diffraction peaks from Ac-Dex is quite different from
529 commercialized polymers such as PLGA, which exhibits strong XRD characterization
530 peaks (Mohammadi et al., 2010). This phenomenon is likely because the Ac-Dex was
531 collected by rapid precipitation in water, which prevents the formation of large polymer
532 crystallites. Strong peaks were present for raw CUR indicating that it was in crystalline
533 form prior to spray drying. XRD diffractograms of the physical mixture, CUR nCmP and
534 CUR MP were absent of any diffraction peaks corresponding to raw CUR, which was
535 due to the dilution effect of Ac-Dex. The results obtained from the XRD diffractograms
536 confirmed those from DSC thermograms, which show that raw CUR was converted to
537 amorphous forms during the particle manufacturing process.

538

539 *3.3.7 In Vitro Aerosol Dispersion Performance Using Next Generation Impactor (NGI)*

540 *In vitro* aerosol dispersion performance properties of the nCmP were evaluated
541 using a Next Generation Impactor™ coupled with a human DPI device (**Figure 6 and**
542 **Figure 7**). The results indicated that the formulated nCmP and MP are favorable for
543 efficient dry powder aerosolization and effective targeted pulmonary delivery. The
544 experimental mass mean aerodynamic diameter ($MMAD_E$) values of all particle systems
545 were approximately 2 μm, while the geometric standard deviation (GSD) values were 2 -
546 3 μm. The $MMAD_E$ values were within the range of 1 - 5 μm that is required for

predominant deposition of particles into the deep lung region (Meenach et al., 2013b), which would be desirable to deliver therapeutics for the treatment of both local and systematic diseases through the lung. The theoretical mass mean aerodynamic diameter ($MMAD_T$, **Table 2**), calculated using the geometric diameter and tapped density, was lower than the experimental MMAD. This discrepancy is likely due to particle agglomeration, which increased the geometric size of the dry powder particulates. All of the particle systems exhibited low tapped density values, which supports the hypothesis that the particles are likely hollow. This can also be attributed to their wrinkled surface morphology, as seen in SEM analysis. The GSD values were within the range of those previously reported and the respirable fraction (RF), fine particle fraction (FPF), and emitted dose (ED) values were all higher than reports from similar systems (Meenach et al., 2013a; Meenach et al., 2013b; Ungaro et al., 2006). The formulated Ac-Dex particle systems are expected to achieve an improved therapeutic effect with a reduced amount of payloads by effectively delivering drugs into the deep lung region.

4. CONCLUSIONS

Two types of pulmonary delivery systems were successfully formulated using Ac-Dex with two different degradation rates. The resulting CUR MP were wrinkled spheres (approximately 1 μm), while nCmP were similar in size with wrinkled surfaces that showed the presence of nanoparticles. The variations in the drug release rates from the Ac-Dex particles were influenced by the Ac-Dex reaction time, ratio of two types of Ac-Dex, and the particle size, which could be easily tuned during the manufacturing process. The pH value of the environment also had a significant influence on the release profiles,

allowing the Ac-Dex particles to release the payload in a controlled fashion. All nCmP and MP systems exhibited desirable properties as dry powder inhalation formulations, including small aerodynamic diameters, which is suitable for deep lung delivery, low water content, which is favorable for particle storage, and amorphization of a crystalline payload, which improves the efficiency of drug dissolution. Overall, the engineered Ac-Dex aerosol particle systems have the potential for targeted delivery of therapeutics into the deep lung.

ACKNOWLEDGEMENTS

The authors gratefully acknowledge financial support from an Institutional Development Award (IDeA) from the National Institute of General Medical Sciences of the National Institutes of Health under grant number P20GM103430. The content is solely the responsibility of the authors and does not necessarily represent the official views of the National Institutes of Health. This material is based upon work conducted at a Rhode Island NSF EPSCoR research facility, supported in part by the National Science Foundation EPSCoR Cooperative Agreement #EPS-1004057. In addition, this material is based in part upon work supported by the National Science Foundation under grant number #1508868. Any opinions, findings, and conclusions or recommendations expressed in this material are those of the authors and do not necessarily reflect the view of the National Science Foundation. Finally, the authors thank RI-INBRE for UPLC access and RIN2 for SEM, DLS, PXRD, and DSC access.

AUTHOR DISCLOSURE STATEMENT

No conflicts of interest exist.

REFERENCES

Akl, M.A., Kartal-Hodzic, A., Oksanen, T., Ismael, H.R., Afouna, M.M., Yliperttula, M., Samy, A.M., Viitala, T., 2016. Factorial design formulation optimization and in vitro characterization of curcumin-loaded PLGA nanoparticles for colon delivery. Journal of Drug Delivery Science and Technology 32, Part A, 10-20.

Atalar, I., Dervisoglu, M., 2015. Optimization of spray drying process parameters for kefir powder using response surface methodology. LWT - Food Science and Technology 60, 751-757.

Bachelder, E.M., Beaudette, T.T., Broaders, K.E., Dashe, J., Fréchet, J.M.J., 2008. Acetal-Derivatized Dextran: An Acid-Responsive Biodegradable Material for Therapeutic Applications. Journal of the American Chemical Society 130, 10494-10495.

Belotti, S., Rossi, A., Colombo, P., Bettini, R., Rekkas, D., Politis, S., Colombo, G., Balducci, A.G., Buttini, F., 2015. Spray-dried amikacin sulphate powder for inhalation in cystic fibrosis patients: The role of ethanol in particle formation. European Journal of Pharmaceutics and Biopharmaceutics 93, 165-172.

Bohrey, S., Chourasiya, V., Pandey, A., 2016. Polymeric nanoparticles containing diazepam: preparation, optimization, characterization, in-vitro drug release and release kinetic study. Nano Convergence 3, 1-7.

Broaders, K.E., Cohen, J.A., Beaudette, T.T., Bachelder, E.M., Fréchet, J.M.J., 2009. Acetalated dextran is a chemically and biologically tunable material for particulate immunotherapy. Proceedings of the National Academy of Sciences 106, 5497-5502.

Cohen, J.A., Beaudette, T.T., Cohen, J.L., Broaders, K.E., Bachelder, E.M., Frechet, J.M., 2010. Acetal-modified dextran microparticles with controlled degradation kinetics and surface functionality for gene delivery in phagocytic and non-phagocytic cells. Advanced materials (Deerfield Beach, Fla.) 22, 3593-3597.

Collier, M.A., Peine, K.J., Gautam, S., Oghumu, S., Varikuti, S., Borteh, H., Papenfuss, T.L., Sataoskar, A.R., Bachelder, E.M., Ainslie, K.M., 2016. Host-mediated Leishmania donovani treatment using AR-12 encapsulated in acetalated dextran microparticles. Int J Pharm 499, 186-194.

Costa, P., Sousa Lobo, J.M., 2001. Modeling and comparison of dissolution profiles. European Journal of Pharmaceutical Sciences 13, 123-133.

Cui, L., Cohen, J.A., Broaders, K.E., Beaudette, T.T., Frechet, J.M., 2011. Mannosylated dextran nanoparticles: a pH-sensitive system engineered for immunomodulation through mannose targeting. Bioconjugate chemistry 22, 949-957.

Gu, B., Linehan, B., Tseng, Y.-C., 2015. Optimization of the Büchi B-90 spray drying process using central composite design for preparation of solid dispersions. International Journal of Pharmaceutics 491, 208-217.

637 He, C., Hu, Y., Yin, L., Tang, C., Yin, C., 2010. Effects of particle size and surface
638 charge on cellular uptake and biodistribution of polymeric nanoparticles. Biomaterials 31,
639 3657-3666.
640 Heyder, J., 2004. Deposition of Inhaled Particles in the Human Respiratory Tract and
641 Consequences for Regional Targeting in Respiratory Drug Delivery. Proceedings of the
642 American Thoracic Society 1, 315-320.
643 Hickey, A.J., Mansour, H.M., Telko, M.J., Xu, Z., Smyth, H.D., Mulder, T., McLean, R.,
644 Langridge, J., Papadopoulos, D., 2007. Physical characterization of component particles
645 included in dry powder inhalers. I. Strategy review and static characteristics. J Pharm Sci
646 96, 1282-1301.
647 Hoang, K.V., Borteh, H.M., Rajaram, M.V., Peine, K.J., Curry, H., Collier, M.A.,
648 Homsy, M.L., Bachelder, E.M., Gunn, J.S., Schlesinger, L.S., Ainslie, K.M., 2014.
649 Acetalated dextran encapsulated AR-12 as a host-directed therapy to control Salmonella
650 infection. Int J Pharm 477, 334-343.
651 Jensen, D.M., Cun, D., Maltesen, M.J., Frokjaer, S., Nielsen, H.M., Foged, C., 2010.
652 Spray drying of siRNA-containing PLGA nanoparticles intended for inhalation. Journal
653 of controlled release : official journal of the Controlled Release Society 142, 138-145.
654 Kamaly, N., Yameen, B., Wu, J., Farokhzad, O.C., 2016. Degradable Controlled-Release
655 Polymers and Polymeric Nanoparticles: Mechanisms of Controlling Drug Release.
656 Chemical Reviews 116, 2602-2663.
657 Kanthamneni, N., Sharma, S., Meenach, S.A., Billet, B., Zhao, J.-C., Bachelder, E.M.,
658 Ainslie, K.M., 2012. Enhanced stability of horseradish peroxidase encapsulated in
659 acetalated dextran microparticles stored outside cold chain conditions. International
660 Journal of Pharmaceutics 431, 101-110.
661 Kauffman, K.J., Kanthamneni, N., Meenach, S.A., Pierson, B.C., Bachelder, E.M.,
662 Ainslie, K.M., 2012. Optimization of rapamycin-loaded acetalated dextran microparticles
663 for immunosuppression. International Journal of Pharmaceutics 422, 356-363.
664 Kho, K., Cheow, W.S., Lie, R.H., Hadinoto, K., 2010. Aqueous re-dispersibility of spray-
665 dried antibiotic-loaded polycaprolactone nanoparticle aggregates for inhaled anti-biofilm
666 therapy. Powder Technology 203, 432-439.
667 Lai, S.K., Wang, Y.-Y., Hanes, J., 2009. Mucus-penetrating nanoparticles for drug and
668 gene delivery to mucosal tissues. Advanced drug delivery reviews 61, 158-171.
669 Mansour, H.M., Rhee, Y.-S., Wu, X., 2009. Nanomedicine in pulmonary delivery.
670 International journal of nanomedicine 4, 299-319.
671 Meenach, S.A., Anderson, K.W., Zach Hilt, J., McGarry, R.C., Mansour, H.M., 2013a.
672 Characterization and aerosol dispersion performance of advanced spray-dried
673 chemotherapeutic PEGylated phospholipid particles for dry powder inhalation delivery in
674 lung cancer. European Journal of Pharmaceutical Sciences 49, 699-711.
675 Meenach, S.A., Kim, Y.J., Kauffman, K.J., Kanthamneni, N., Bachelder, E.M., Ainslie,
676 K.M., 2012. Synthesis, Optimization, and Characterization of Camptothecin-Loaded
677 Acetalated Dextran Porous Microparticles for Pulmonary Delivery. Molecular
678 Pharmaceutics 9, 290-298.
679 Meenach, S.A., Vogt, F.G., Anderson, K.W., Hilt, J.Z., McGarry, R.C., Mansour, H.M.,
680 2013b. Design, physicochemical characterization, and optimization of organic solution
681 advanced spray-dried inhalable dipalmitoylphosphatidylcholine (DPPC) and
682 dipalmitoylphosphatidylethanolamine poly(ethylene glycol) (DPPE-PEG) microparticles

and nanoparticles for targeted respiratory nanomedicine delivery as dry powder inhalation aerosols. International journal of nanomedicine 8, 275-293.
Mohammadi, G., Valizadeh, H., Barzegar-Jalali, M., Lotfipour, F., Adibkia, K., Milani, M., Azhdarzadeh, M., Kiafar, F., Nokhodchi, A., 2010. Development of azithromycin-PLGA nanoparticles: physicochemical characterization and antibacterial effect against Salmonella typhi. Colloids and surfaces. B, Biointerfaces 80, 34-39.
Rasband, W.S., 1997-2016. ImageJ.
Seidlitz, A., Weitschies, W., 2012. In-vitro dissolution methods for controlled release parenterals and their applicability to drug-eluting stent testing. The Journal of pharmacy and pharmacology 64, 969-985.
Shuwisitkul, D., 2011. title., Freie Universität Berlin.
Sung, J.C., Padilla, D.J., Garcia-Contreras, L., Verberkmoes, J.L., Durbin, D., Peloquin, C.A., Elbert, K.J., Hickey, A.J., Edwards, D.A., 2009. Formulation and pharmacokinetics of self-assembled rifampicin nanoparticle systems for pulmonary delivery. Pharm Res 26, 1847-1855.
Takashima, Y., Saito, R., Nakajima, A., Oda, M., Kimura, A., Kanazawa, T., Okada, H., 2007. Spray-drying preparation of microparticles containing cationic PLGA nanospheres as gene carriers for avoiding aggregation of nanospheres. Int J Pharm 343, 262-269.
Tomoda, K., Ohkoshi, T., Kawai, Y., Nishiwaki, M., Nakajima, T., Makino, K., 2008. Preparation and properties of inhalable nanocomposite particles: effects of the temperature at a spray-dryer inlet upon the properties of particles. Colloids and surfaces. B, Biointerfaces 61, 138-144.
Ulery, B.D., Nair, L.S., Laurencin, C.T., 2011. Biomedical Applications of Biodegradable Polymers. Journal of polymer science. Part B, Polymer physics 49, 832-864.
Ungaro, F., De Rosa, G., Miro, A., Quaglia, F., La Rotonda, M.I., 2006. Cyclodextrins in the production of large porous particles: Development of dry powders for the sustained release of insulin to the lungs. European Journal of Pharmaceutical Sciences 28, 423-432.
Vehring, R., 2008. Pharmaceutical Particle Engineering via Spray Drying. Pharm Res 25, 999-1022.
W, F., 2008. The ARLA Respiratory Deposition Calculator.
Wang, Z., Cuddigan, J.L., Gupta, S.K., Meenach, S.A., 2016. Nanocomposite Microparticles (nCmP) for the Delivery of Tacrolimus in the Treatment of Pulmonary Arterial Hypertension. International Journal of Pharmaceutics 512, 305-313.
Wang, Z., Meenach, S.A., 2016. Synthesis and Characterization of Nanocomposite Microparticles (nCmP) for the Treatment of Cystic Fibrosis-Related Infections. Pharmaceutical Research 33, 1862-1872.
Wu, L., Miao, X., Shan, Z., Huang, Y., Li, L., Pan, X., Yao, Q., Li, G., Wu, C., 2014. Studies on the spray dried lactose as carrier for dry powder inhalation. Asian Journal of Pharmaceutical Sciences 9, 336-341.
Wu, X., Zhang, W., Hayes, D., Jr., Mansour, H.M., 2013. Physicochemical characterization and aerosol dispersion performance of organic solution advanced spray-dried cyclosporine A multifunctional particles for dry powder inhalation aerosol delivery. Int J Nanomedicine 8, 1269-1283.

TABLES AND FIGURES

Table 1. Average diameter (as measured by dynamic light scattering), polydispersity index (PDI), and zeta potential (ZP) of CUR-loaded nanoparticles before spray drying (NP) and after redispersion from nanocomposite microparticles (nCmP) (mean ± standard deviation, n = 3).

Particle System	Average Diameter (nm)	PDI	ZP (mV)
NP-5min	192.2 ± 2.7	0.07 ± 0.03	-8.4 ± 4.1
NP-h	201.1 ± 1.5	0.02 ± 0.01	-8.0 ± 3.7
NP-3h	206.1 ± 1.3	0.03 ± 0.03	-7.0 ± 1.6
nCmP-5min	199.3 ± 1.3	0.09 ± 0.02	-14.5 ± 1.0
nCmP-h	210.2 ± 2.5	0.07 ± 0.01	-13.3 ± 1.9
nCmP-3h	213.5 ± 2.4	0.02 ± 0.00	-11.2 ± 1.6

Table 2. Geometric diameter (as measured by SEM imaging and ImageJ analysis), experimental mass median aerodynamic diameter ($MMAD_E$), geometric standard deviation (GSD), water content, tapped density, theoretical mean mass aerodynamic diameter ($MMAD_T$), drug loading, and drug encapsulation efficiency (EE) of nCmP and MP (mean ± standard deviation, n = 3).

Particle System	Geometric Diameter (µm)	$MMAD_E$ (µm)	GSD (µm)	Water Content (%)	Tapped Density (g/cm^3)	$MMAD_T$ (µm)	Drug Loading (mg/100 mg particle)	EE (%)
nCmP-5min	1.52 ± 0.33	1.61 ± 0.16	2.37 ± 0.24	7.69 ± 0.76	0.122 ± 0.001	0.52 ± 0.09	0.57± 0.006	28.7 ± 0.32
nCmP-h	1.77 ± 0.46	2.05 ± 0.09	2.62 ± 0.17	7.89 ± 1.56	0.115 ± 0.004	0.60 ± 0.09	0.58 ± 0.008	28.4 ± 0.42
nCmP-3h	1.72 ± 0.39	1.89 ± 0.09	2.70 ± 0.13	7.86 ± 0.43	0.133 ± 0.002	0.64 ± 0.12	0.62 ± 0.013	31.2 ± 0.63
MP-5min	0.89 ± 0.30	2.38 ± 0.06	2.14 ± 0.14	6.12 ± 1.33	0.050 ± 0.001	0.21 ± 0.03	1.33 ± 0.092	66.3 ± 4.62
MP-h	1.26 ± 0.41	2.21 ± 0.23	2.17 ± 0.03	5.87 ± 1.85	0.050 ± 0.001	0.29 ± 0.32	1.03 ± 0.030	51.6 ± 1.48
MP-3h	1.05 ± 0.36	2.41 ± 0.07	2.02 ± 0.08	5.23 ± 1.13	0.052 ± 0.001	0.23 ± 0.03	1.12 ± 0.012	55.8 ± 0.61

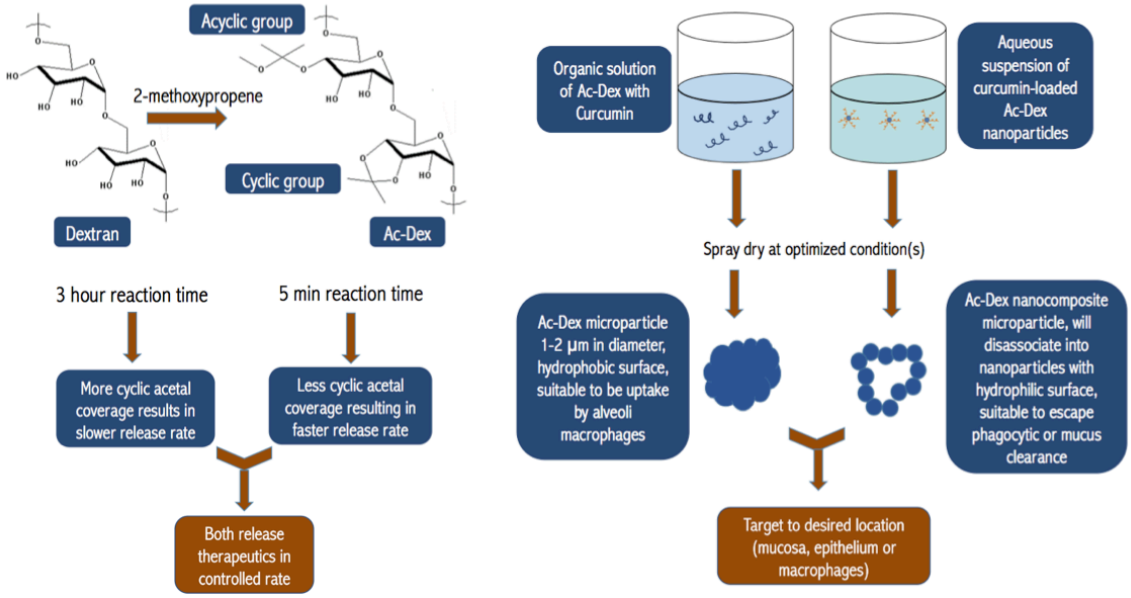

Figure 1. Schematic depicting the synthesis of Ac-Dex (Left) and preparation of nanoparticles and formation of nanocomposite microparticles (nCmP) and microparticles (MP) (Right).

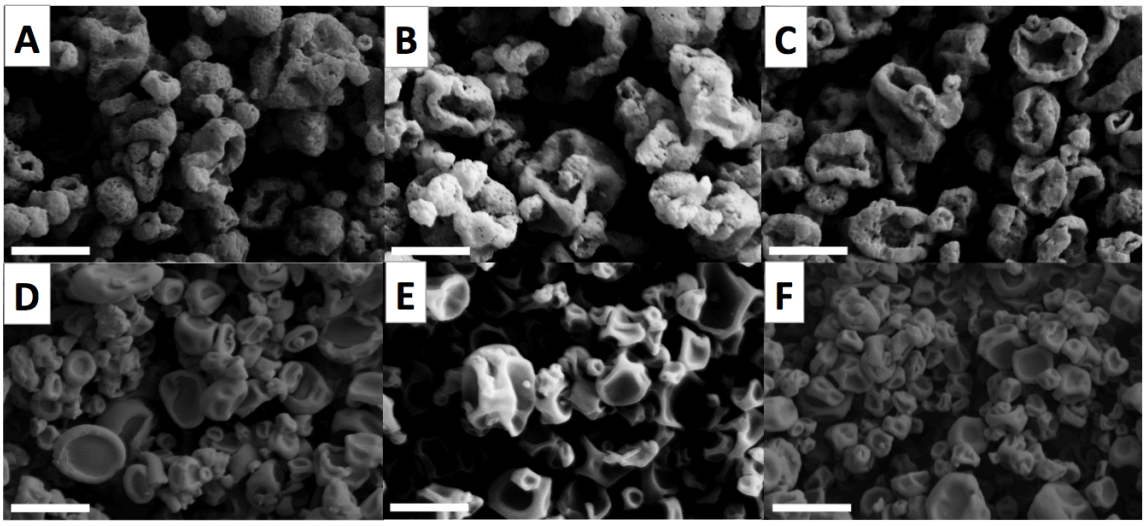

Figure 2. SEM micrographs of curcumin-loaded nanocomposite microparticles (CUR nCmP) and microparticles (CUR MP) including: (A) CUR nCmP-5min, (B) CUR nCmP-h, (C) CUR nCmP-3h, (D) CUR MP-5min, (E) CUR MP-h, and (F) CUR MP-3h systems. Scale bar = 2 µm.

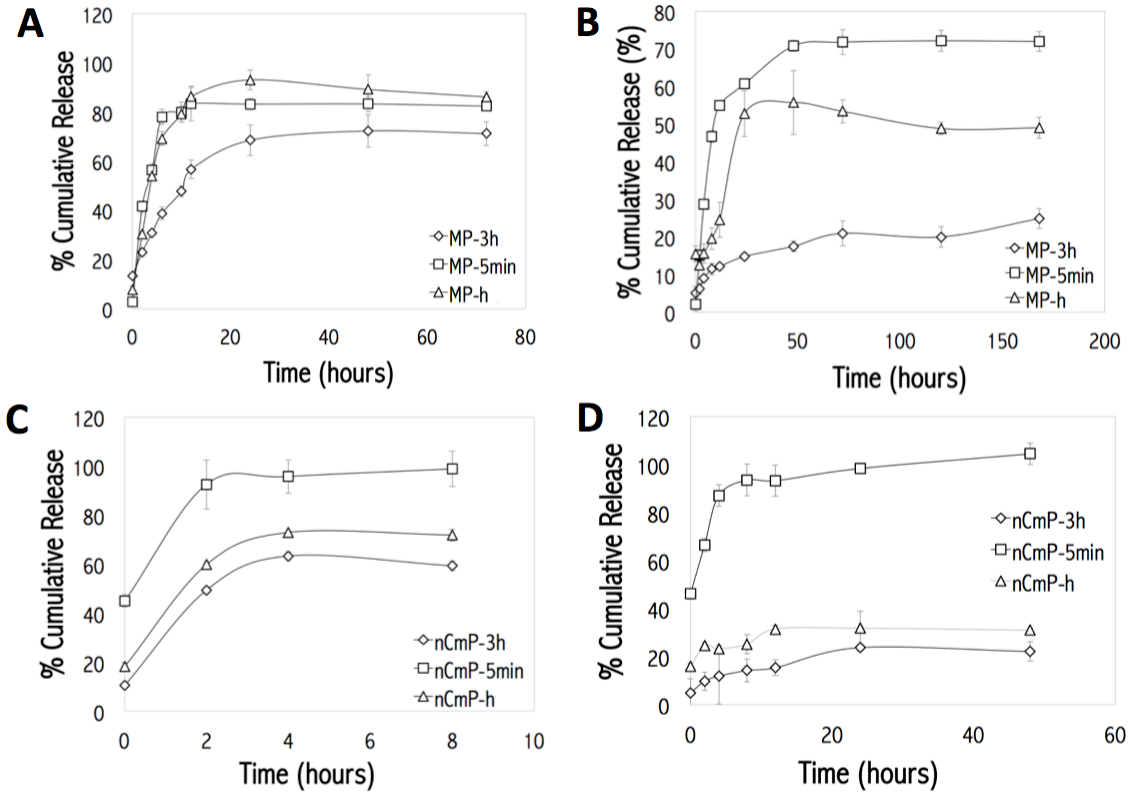

Figure 3. *In vitro* drug release profiles for curcumin-loaded microparticle (MP) systems at (A) pH 5 and (B) pH 7.4 and curcumin-loaded nanocomposite microparticle (nCmP) system at (C) pH 5 and (D) pH 7.4.

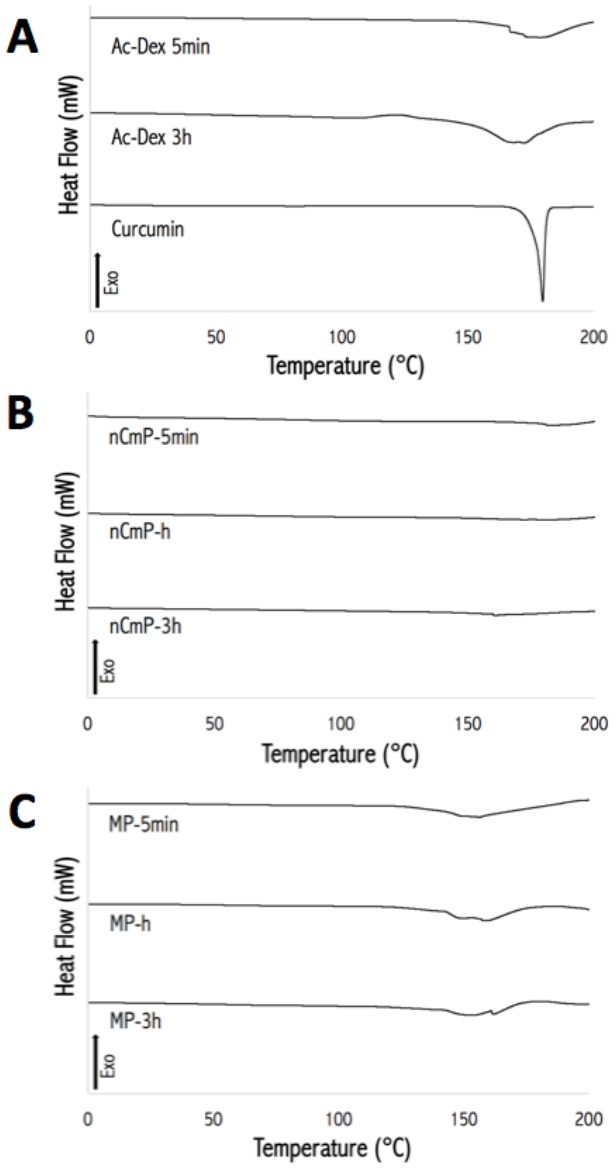

761

762 **Figure 4**. Representative differential scanning calorimetry (DSC) thermograms of (A)
763 raw curcumin (CUR), raw acetalated dextran-5min (Ac-Dex-5min), and raw acetalated
764 dextran-3h (Ac-Dex-3h), (B) CUR nCmP-5min, CUR nCmP-h, and CUR nCmP-3h, and
765 (C) CUR MP-5min, CUR MP-h, and CUR MP-3h.

766

767

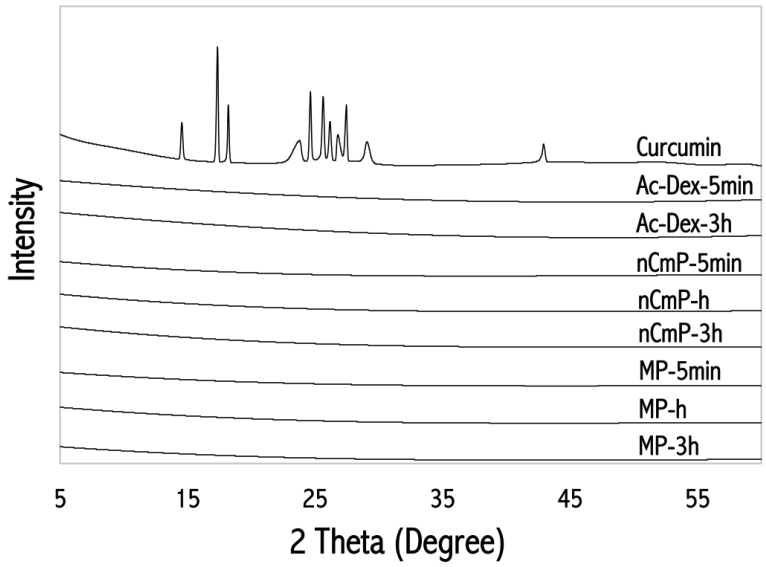

Figure 5. Representative powder X-ray diffractograms (PXRD) of raw curcumin (CUR), raw acetalated dextran-5min (Ac-Dex-5min), raw acetalated dextran-3h (Ac-Dex-3h), CUR nCmP-5min, CUR nCmP-h, CUR nCmP-3h, CUR MP-5min, CUR MP-h, and CUR MP-3h.

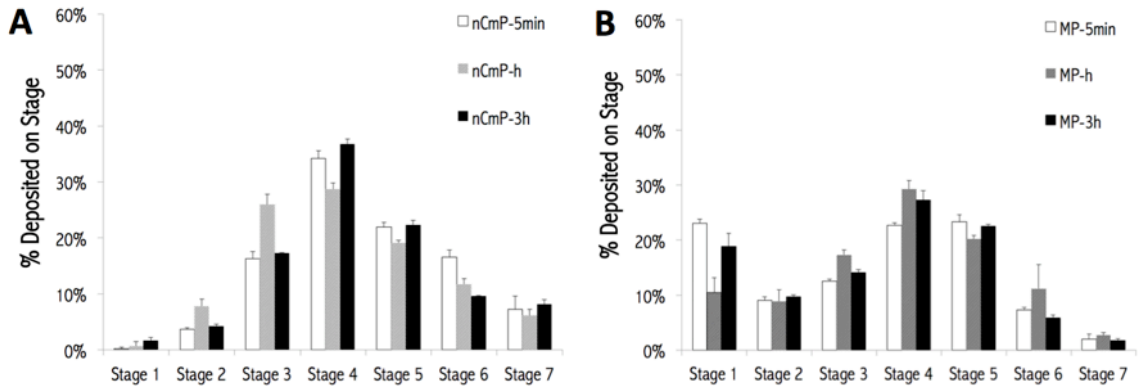

Figure 6. Aerosol dispersion performance of (A) curcumin-loaded nanocomposite microparticles (CUR nCmP) and (B) microparticles (CUR MP) as % particles deposited on each stage of the Next Generation Impactor™ (NGI™). For Q = 60 L/min, the effective cutoff diameters (D_{50}) for each impaction stage are as follows: stage 1 (8.06 μm), stage 2 (4.46 μm), stage 3 (2.82 μm), stage 4 (1.66 μm), stage 5 (0.94 μm), stage 6 (0.55 μm), and stage 7 (0.34 μm) (mean ± standard deviation, n = 3).

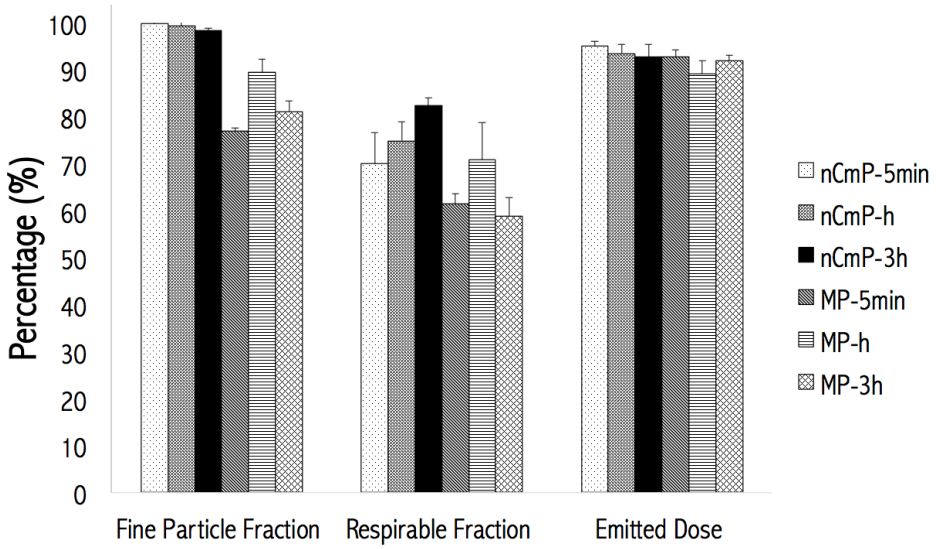

Figure 7. *In vitro* aerosol dispersion performance properties including fine particle dose (FPD), fine particle fraction (FPF), respirable fraction (RF), and emitted dose (ED) for curcumin loaded nanocomposite microparticles (CUR nCmP) and microparticles (CUR MP) (mean ± standard deviation, n = 3).

SUPPLEMENTAL INFORMATION

S.1 Drug Release Model Descriptions

The drug release data of the particle systems was fitted to several relevant models (equations shown below) to aid in the determination of the type of release the systems underwent. For the models that can be linearized (all except for Baker's model), the coefficient of determination (R^2) was calculated to determine the applicability of the release models. For Baker's model, Microsoft Excel with Solver add-in was applied to determine the parameters that minimize the sum of squares of the residues of the model. The models, equations, and their corresponding parameters are as follows:

First order model: $$\log M_t = \log M_0 + \frac{K}{2.303} t \qquad \text{(S1)}$$

where M_t is the amount of drug released at time t, M_0 is the initial amount of drug in the solution, and K is the first order release constant.

Weibull model: $$m = 1 - \exp\left(\frac{-(t - T_i)^b}{a}\right) \qquad \text{(S2)}$$

where m is the accumulated fraction of the drug released at time t, a is the scale parameter, which defines the time scale of the process, T_i is the location parameter, which represents the lag time before the onset of the dissolution or release process, and b is the shape parameter, which characterizes the shape of release curve.

828

829 Higuchi model: $M_t = Kt^{1/2} + b$ (S3)

830

831 where Mt is the amount of drug released at time t, K is the Higuchi dissolution constant,
832 and b is the amount of drug released at time 0.

833

834 Hixson–Crowell model: $W_0^{1/3} - W_t^{1/3} = Kt$ (S4)

835

836 where W_0 is the initial amount of drug in the particles, W_t is the remaining amount of
837 drug in the particles at time t, and K is a constant characterizing the surface to volume
838 relationship.

839

840 Korsmeyer–Peppas model: $m = at^n$ (S5)

841

842 where a is a constant characterizing the structural and geometric properties of the
843 particles, n is the release exponent, indicating the drug release mechanism, and m is the
844 accumulated fraction of the drug released at time t.

845

846 Baker–Lonsdale model: $\frac{3}{2}[1-(1-m)^{2/3}] - m = Kt$ (S6)

847

848 where K is the release constant and m is the accumulated fraction of the drug released at
849 time t.

Hopfenberg model: $m = 1 - [1 - Kt(t-1)]^n$ (S7)

where K is a constant equal to k_0/C_0a_0, where k_0 is the erosion rate constant, C_0 is the initial concentration of drug in the matrix, and a_0 is the initial radius for particles. m is the accumulated fraction of the drug released at time t.

Baker's model: $M_t = A(2P_0e^{kt}C_0t)^{1/2}$ (S8)

where M_t is the amount of drug released in time t, P_0 is the drug permeability, A is the total area of the particle, C_0 is the drug concentration at the initial time, and k is the first-order rate constant of bond cleavage of the polymer carrier.

Table S1. Drug loading and encapsulation efficiency of curcumin NP including NP-5min, NP-h, and NP-3h**.**

Particle System	Drug Loading (mg/100mg particle)	EE (%)
NP-5min	0.600 ± 0.059	30.0 ± 2.95
NP-h	0.621 ± 0.056	31.0 ± 2.82
NP-3h	0.617 ± 0.063	30.9 ± 3.15

Table S2. The release duration and total fraction of curcumin released from each particle system at acidic and neutral pH.

	pH = 5		pH = 7.4	
Particle System	Release Duration (h)	Total Released (%)	Release Duration (h)	Total Released (%)
nCmP-5min	2	92.6	8	93.6
nCmP-h	2	63.4	12	31.5
nCmP-3h	4	73.0	24	23.7
MP-5min	6	78.0	24	60.6
MP-h	12	86.4	24	52.7
MP-3h	24	68.5	168	24.9

Table S3. Summary of the coefficient of determinations (R^2) of all the fitted drug release models for all particle system. The model with relatively high R^2 for all particle systems was regarded as a viable fit for that system.

	pH = 5					
Model	**nCmP - 5min**	**nCmP -h**	**nCmP -3h**	**MP - 5min**	**MP -h**	**MP -3h**
First order	0.7835	0.8549	0.8511	0.5730	0.4848	0.7517
Hixson–Crowell	0.8615	0.9571	0.9613	0.8470	0.8899	0.9490
Higuchi (modified)	0.9468	0.9968	0.9989	0.9867	0.9748	0.9715
Korsmeyer–Peppas	0.9998	0.6906	0.5050	0.8100	0.8843	0.9882
Baker–Lonsdale	0.8729	0.9945	0.9799	0.9065	0.9595	0.9753
Hopfenberg	0.5497	0.8743	0.9029	0.8925	0.849	0.9276
Weibull	0.9098	0.5773	0.2538	0.9387	0.9936	0.9353

	pH = 7.4					
Model	**nCmP - 5min**	**nCmP -h**	**nCmP - 3h**	**MP - 5min**	**MP -h**	**MP -3h**
First order	0.8084	0.7345	0.7574	0.3797	0.8290	0.6414
Hixson–Crowell	0.9312	0.8021	0.9482	0.7696	0.9117	0.8185
Higuchi (modified)	0.9573	0.8758	0.9732	0.9369	0.8288	0.9462
Korsmeyer–Peppas	0.8990	0.5374	0.9457	0.8828	0.9349	0.9708
Baker–Lonsdale	0.9709	0.8172	0.9089	0.9283	0.9141	0.9079
Hopfenberg	0.8493	0.8678	0.9685	0.7462	0.8241	0.8526
Weibull	1.0000	0.5235	0.7905	0.9783	0.8897	0.8963

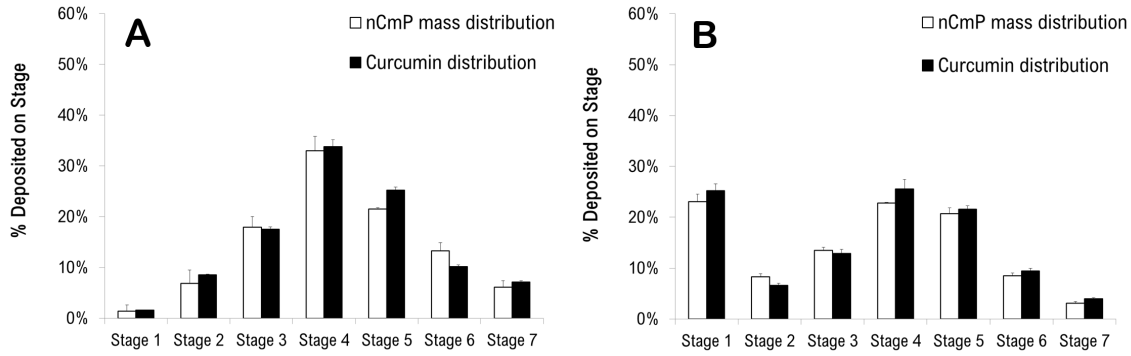

Figure S1. Relationship between particle mass distribution and curcumin (CUR) distribution in all chambers of NGI for (A) CUR-nCmP and (B) CUR-MP.

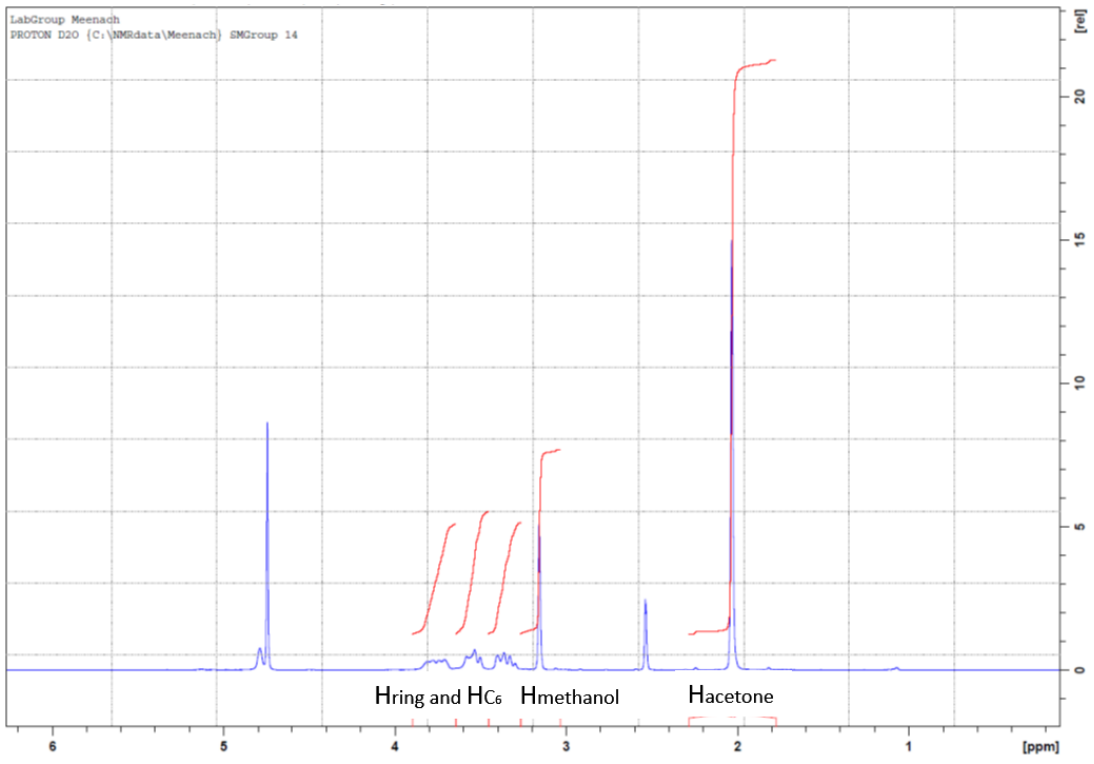

Figure S2. NMR analysis of Ac-Dex where peaks using during analysis include 3.4-4.0 ppm for dextran (H_{ring} and H_{C6}), 3.36 ppm for methanol, and 2.08 ppm for acetone.

Cyclic acetal coverage (CAC) and total conversion of -OH group were calculated by the following equations:

$$\text{Normalization factor } (\text{NF}) = \frac{\text{Total area of 3 dextran peaks}}{6}$$

$$\text{Methanol per glucose} = \frac{\text{Methanol Peak Area}}{3 \times \text{NF}}$$

912

$$\text{Acetone per glucose} = \frac{\text{Acetone Peak Area}}{6 \times \text{NF}}$$

$$\text{Cyclic acetal coverage } (\text{CAC}) = (\text{Acetone per glucose} - \text{Methanol per glucose}) \times 100\%$$

$$\text{Total conversion of } -\text{OH groups} = \frac{(2 \times \text{Acetone per glucose} - \text{Methanol per glucose})}{3} \times 100\%$$

913

914

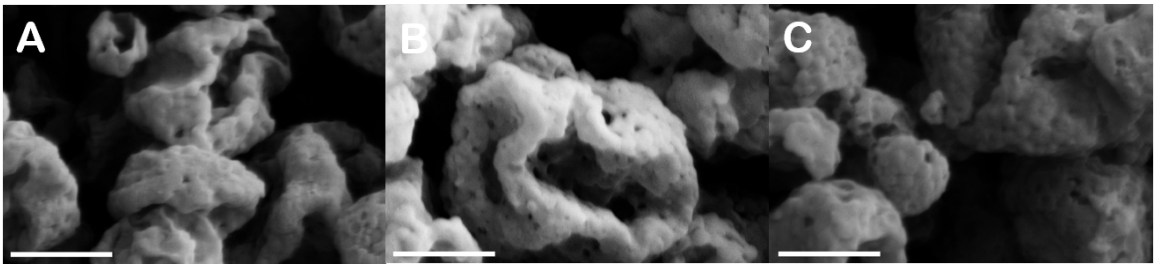

915

916 **Figure S3**. Zoomed in images of CUR-nCmP including: (A) CUR nCmP-5min, (B) CUR
917 nCmP-h, (C) CUR nCmP-3h. Scale bar = 2 μm.

918

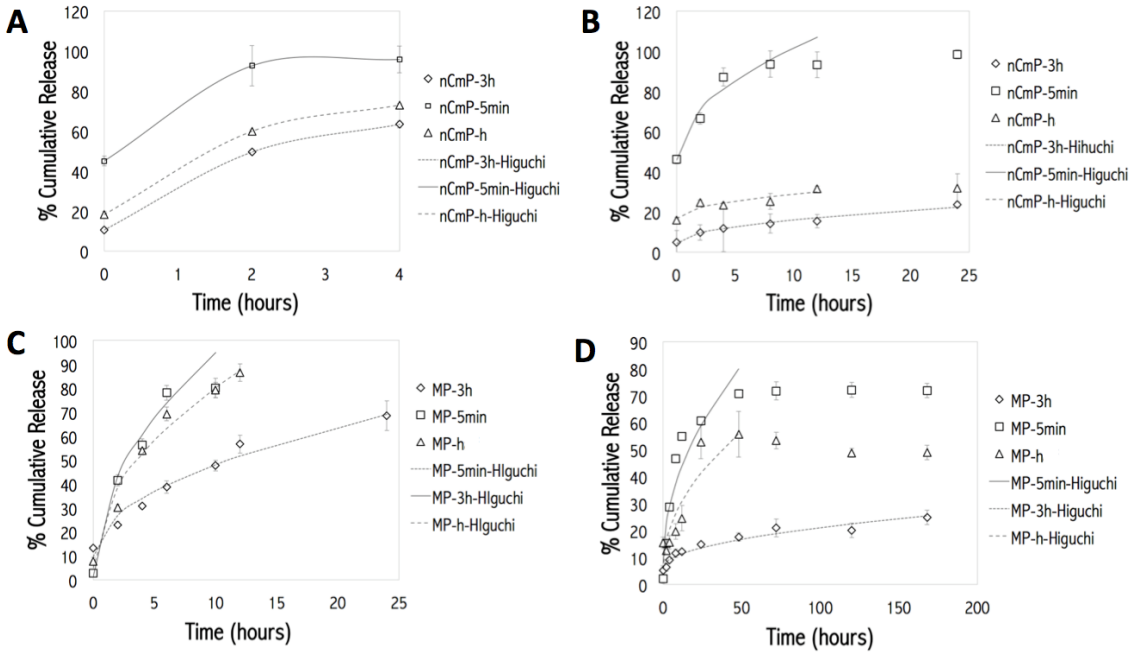

Figure S4. Original data and fitted curves of *in vitro* drug release profiles for curcumin (CUR) nCmP (A and B) and MP systems (C and D) including CUR nCmP-5min, CUR nCmP-h, CUR nCmP-3h, CUR MP-5min, CUR MP-h, and CUR MP-3h at pH = 5 (A and C) and pH = 7.4 (B and D).

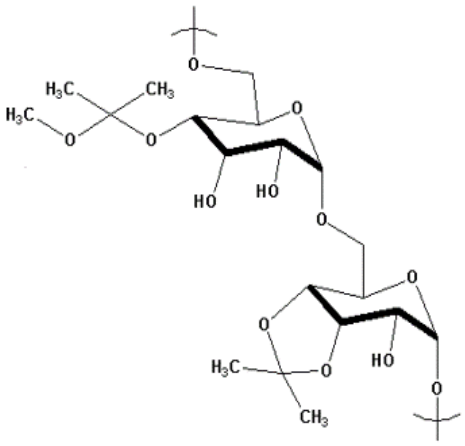

Figure S5. Structure of acetalated dextran (Ac-Dex).